This document is the Accepted Manuscript version of a Published Work that appeared in final form in ***Macromolecules*** 54(4) : 1870-1880 (2021), copyright © 2020 American Chemical Society after peer review and technical editing by the publisher. To access the final edited and published work see https://doi.org/10.1021/acs.macromol.0c02259

Direct Relationship between Dispersion and Crystallization Behavior in Poly(ethylene oxide)/Poly(ethylene glycol)-*g*-Silica Nanocomposites

Xiangning Wen,[a,b] Yunlan Su,[a,b*] Guoming Liu,[a,b] Shaofan Li,[a,b] Alejandro J. Müller,[c,d*] Sanat K. Kumar,[e] Dujin Wang[a,b]

[a] Key Laboratory of Engineering Plastics, CAS Research/Education Center for Excellence in Molecular Sciences, Institute of Chemistry, Chinese Academy of Sciences, Beijing 100190, China

[b] University of Chinese Academy of Sciences, Beijing 100049, China

[c] POLYMAT and Faculty of Chemistry, University of the Basque Country UPV/EHU, Paseo Manuel de Lardizabal 3, 20018 Donostia-San Sebastián, Spain

[d] IKERBASQUE, Basque Foundation for Science, Bilbao, Spain

[e] Department of Chemical Engineering, Columbia University, New York, New York 10027, United States

ABSTRACT

The inclusion of polymer-grafted nanoparticles (PGNPs) can impart various functional properties to polymer nanocomposites (PNCs). For semicrystalline polymers, we can control the spatial dispersion of PGNPs and presumably use it to modulate the nucleation rate of the polymer. In this work, the correlation between the dispersion quality of poly(ethylene glycol) (PEG) grafted silica (PEG-*g*-SiO_2) nanoparticles and the crystallization ability of poly(ethylene oxide) (PEO) nanocomposites is systematically investigated by varying the grafting density (σ, chains/nm^2) and the value of *P/N* (*P*: molecular weight of matrix chains, *N*: molecular weight of grafted chains). The variation of PEG-*g*-SiO_2 dispersion state was studied by morphological characterization and small-angle X-ray scattering (SAXS). It was found that, in contrast to the unmodified SiO_2 and poly(methyl methacrylate) grafted silica (PMMA-*g*-SiO_2), PEG-*g*-SiO_2 (high σ and low *P/N*) can increase the nucleation rate of PEO even under conditions where they are well dispersed in the PEO matrix. Evidently, the nature of the graft, i.e., amorphous PMMA vs. crystallizable PEO, has profound consequences in this context, a novel result that has not been anticipated based on previous work. NP aggregation occurs at higher *P/N* values and limits the effectiveness of the grafted PEG on the crystallization ability of PEO nanocomposites. Based on differential scanning calorimetry (DSC) and polarized light optical microscopy (PLOM) characterization, we deduced that the increased nucleation density at high σ and low *P/N* has a strong impact on accelerating the overall crystallization of PEO nanocomposites.

Keywords: Crystallization, Poly(ethylene oxide), Polymer grafted nanoparticles, Nanocomposites

1. INTRODUCTION

The performance of polymeric materials can be enhanced by the addition of nanoparticles (NPs).[1-5] However, the irreversible aggregation of bare NPs within the polymer matrix often impairs property enhancements of these polymer nanocomposites (PNCs). This is an issue because of the immiscibility between inorganic NPs and the organic polymer chains.[6-8] Achieving good NPs dispersion is therefore vital to fully exploit the potentially excellent properties of PNCs.[9] In this scenario, grafting polymer chains onto the surface of NPs has been used as a promising strategy to control NP dispersion in PNCs.[3, 10-12]

The spatial distribution of polymer-grafted nanoparticles (PGNPs) in a polymer matrix can be tuned by regulating the interactions between the grafted chains and the polymer matrix. The following parameters must thus be carefully controlled: grafting density (σ), chain length ratio of matrix (P) to grafted polymer (N), NPs sizes, as well as the chemical properties of grafted polymer.[13-14] A comprehensive morphology phase diagram of PGNPs in PNCs obtained from the available data within the recent literature has been summarized by Kumar et al.,[6] in which the dispersion regions are sensitively affected by changes in σ and P/N.

Chevigny et al.[15] found that the dispersion mechanism of polystyrene grafted SiO_2 (PS-*g*-SiO_2) in a PS matrix is closely related to the P/N ratio. Grafted NPs separate from the PS matrix and form compact aggregates when $P/N > 4.2$, whereas for $P/N < 4.2$ they are individually dispersed. On the other hand, Srivastava et al.[7] found that changing σ from moderate to high values (0.8 chains/nm^2 to 1.25

chains/nm^2) and employing a *P/N* ratio lower than 5, allowed for poly(ethylene glycol) grafted SiO_2 (PEG-*g*-SiO_2) to be well-dispersed in a PEG matrix.

This current work is motivated by the conjecture that the factors influencing the spatial distribution of PGNPs could also determine the mechanism and the kinetics of polymer crystallization in semicrystalline PNCs.[16] A recent study has shown that polyethylene grafted maghemite NPs (PE-*g*-maghemite) can be well-dispersed in a PE matrix at any *P/N* ratio, providing the PNCs with excellent thermomechanical properties and crystallization ability.[17] The incorporation of longer grafted chains in poly(L-lactic acid) grafted silica (PLLA-*g*-SiO_2) has been found to increase the nucleating effect of these PGNPs on the PLLA matrix even at low σ.[18] In contrast to these findings, Jimenez et al.[19] studied the crystallization behavior of PEO when it is well-mixed with poly(methyl methacrylate) grafted NPs (PMMA-*g*-SiO_2); these authors found that the grafted NPs decreased crystal growth rate and reduced the crystallinity of PEO at higher NPs contents. The current understanding is that these reductions come from two sources – the increase in viscosity on the addition of NPs, and the confinement effects imposed on the polymer melts due to the presence of the NPs; both of these effects slow down chain motion to the growing crystal front. In contrast, crystal nucleation was not significantly affected. They also reported that at high enough crystallization temperatures, PMMA-*g*-SiO_2 NPs are selectively moved into interlamellar, interfibrillar, and interspherulitic zones of the lamellar PEO morphology.[20]

Well-dispersed bare silica NPs in a PEO matrix[21], and silica NPs with a PMMA

long brush and a dense short polystyrene (PS) brush,[22] which display a range of self-assembled morphologies in the melt state, also showed that growth rates are reduced in the nanocomposites. However, the rate of nucleation showed much more complicated behavior in these cases. While the bimodal grafted NPs always reduced nucleation rates, the bare NPs reduced crystallization rates under some conditions but not others.[21] It is thus safe to conclude that, while there is considerable understanding of the growth of polymer spherulites in the presence of the NPs, the corresponding understanding of nucleation is still nascent.

Therefore, the main purpose of this work is to establish the relationship between the state of NP dispersion and the crystal nucleation and growth of the matrix PEO. This control is achieved by variations of σ and P/N in PNCs containing PGNPs. Poly(ethylene oxide) (PEO) is a well-studied semicrystalline polymer,[23-24] and PEO/silica PNCs are also interesting for solid polymer electrolytes[25-26]. With the goal of systematically studying the crystallization behavior of semicrystalline PNCs, we prepared PEG grafted SiO_2 (PEG-*g*-SiO_2) via the "grafting to" method[27] over a range of molecular weights (M_n = 4k g·mol^{-1}, M_n = 5k g·mol^{-1} and M_n = 10k g·mol^{-1}) at different grafting densities (σ = 0.3, 0.46 and 0.73 chains/nm^2, respectively). Our results show that the dispersion of PEG-*g*-SiO_2 has a crucial effect on the crystallization behavior of PEO nanocomposites. PEG-*g*-SiO_2 can act as an effective nucleating agent in the case of higher σ and lower P/N, which correspond to the well-dispersed NP states of PEO nanocomposites. These studies should be contrasted with the earlier work where the grafts themselves are non-crystalline, and suggest that

the nature of the polymers at the surface (i.e., amorphous vs. crystalline), apparently, can lead to either reduced or increased nucleation rates. These results therefore point to a relatively straightforward means to control the nucleation rate of semicrystalline polymer hosts.

2. EXPERIMENTAL

Materials

Methoxy polyethylene glycol (MPEG) with molecular weights M_n = 4k g·mol^{-1}, 5k g·mol^{-1} and 10k g·mol^{-1}, respectively, were purchased from TCI (Tokyo, Japan). Monodisperse spherical silica NPs, mean diameter $2R_c = 50$ nm, were prepared by the method of Stöber and Fink.[28] N-(2-aminoethy)-3-aminopropylmethyldimethoxysilane (ADMS) was purchased from Alfa Aesar Co., Shanghai, China. Poly(ethylene oxide) (PEO) with different molecular weights (1.7k, 5k, 7.8k, 20k, 35k, 95k g·mol^{-1}, respectively) were purchased form Polymer Source, Inc.

Sample Preparation

Monodisperse SiO_2 were separately grafted with PEG chains of M_n = 4k g·mol^{-1}, 5k g·mol^{-1} and 10k g·mol^{-1}, respectively, in a series of experiments. We examined different grafting densities (σ values in chains/nm^2 were calculated by TGA, as shown in Figure S1 of the Supporting Information, SI) achieved using the "grafting to" method, as has been reported in our previous study.[29] For clarity, the PEG grafted SiO_2 was denoted as PEG*x*-*g*-SiO_2-*y*, where *x* represents the molecular weight of

grafted PEG and *y* represents the grafting density.

To prepare the PEO/PEG-*g*-SiO_2 nanocomposites, PEO and PEG-*g*-SiO_2 were individually dispersed in acetonitrile and then mixed in the desired volume ratios. The mixtures were sonicated for 5 min and then stirred for about 6 h at room temperature, before casting onto Petri dishes. The nanocomposites were dried under a fume hood for 24 h to remove the solvent.

Characterization

Small Angle X-ray Scattering

Small-angle X-ray (SAXS) scattering was carried out on a Xeuss 2.0 SAXS/WAXS System (Xenocs, France) with λ_{Cu} = 0.154 nm at 100 ℃, i.e., the measurements were performed with the polymer matrix in the melt. Two dimensional (2D) SAXS patterns were collected with a Pilatus detector (Switzerland), having a resolution of 487 × 619 pixels (pixel size = 172 ×172 μm). The sample-to-detector distance was 2508 mm, and the calibration was performed with a Silver Behenate ($AgC_{22}H_{43}O_2$) standard.

In order to extract the information of the interparticle correlation at lower q region, another SAXS with longer sample-to-detector distance (6000 mm) was carried out on a Xeuss 2.0 SAXS/WAXS System (Xenocs, France) with λ_{Cu}= 0.154 nm at 100 ℃ at the Changchun Institute of Applied Chemistry Academy of Science (CIAC). 2D SAXS patterns were transformed into 1D intensity profiles through the Fit2D software.

Transmission Electron Microscope (TEM)

The morphology of the PEO nanocomposites was observed by cryo-TEM Themis 300. The specimen was prepared by Thermo scientific Vitrobot in a closed chamber with 70 % relative humidity and a fixed temperature of 22 ºC. First, a 2.5 µl droplet of the molten samples was dripped onto a perforated carbon film-supported grid held by tweezers and pre-equilibrated for 1 s, producing a thin liquid film spanning the holes of the grid. The grid was then quickly plunged into liquid nitrogen to create the vitrified sample (presumably without crystallization). Micrographs were recorded by Themis 300 using an operating voltage of 300 kV.

Thermogravimetric Analysis

The grafting density of PEO was calculated by thermogravimetric analysis (TGA, PE8000, USA). 2-3 mg samples were heated from 50 to 100 ℃ at a rate of 40 ℃/min and held for 2 min at 100 ℃ to remove physically adsorbed water, then heated from 100 to 800 ℃ with a rate of 20 ℃/min.

Differential Scanning Calorimetry

A TA-Q2000 DSC apparatus was employed to study the crystallization behavior of the PEO nanocomposites. The equipment was calibrated with indium and tin standards. The samples (3-5 mg) were encapsulated in Aluminium pans, and ultra-pure nitrogen was used as a purge gas. First, the samples were heated to 100 ℃ and held for 3 min to erase any thermal history. Second, they were cooled to -60 ℃, and finally, reheated to 100 ℃. All tests were performed at a cooling and heating rate of 20 ℃/min. The peak temperatures of the obtained crystallization exotherms (T_c) were recorded.

Dynamic Light scattering

Dynamic light scattering (DLS) measurements were performed at 25 ℃ using a Malvern Zetasizer nano-S to obtain the size of the grafted PEG. PEG grafted SiO_2 NPs were dispersed in ethanol (10 ml) at a fixed concentration of 0.1 mg/ml. The reported results are the average of three replicates.

Polarized Light Optical Microscope

A polarized light optical microscope (PLOM, Olympus BX51) equipped with a Linkam THMS600 temperature controller was employed for the observation of the crystalline morphology. The samples were sandwiched between two cover glasses and heated to 100 ℃ for 5 min. Then the samples were cooled at 20 ℃/min (the same cooling rate employed in the DSC runs) to 25 ℃.

3. RESULTS AND DISCUSSION

3.1. Size of the grafted PEG chains

Dynamic light scattering (DLS) provides an efficient way to study the structure and scaling behavior of the tethered chains, and to understand how the grafted chains interact with the matrix chains.[30-31] The thicknesses of the grafted chains can reflect structural properties that are closely related to the grafting density and molecular weight of the grafted polymer.[30]

Table 1 presents the brush height, h, obtained from DLS (as shown in Figure S2-S3 of the SI) for the PEG-*g*-SiO_2 NPs with different σ and M_n in dilute solution as

discussed above. The brush height is defined as $h = R_h - R_c$, where R_h is the hydrodynamic radius of the PEG-*g*-SiO_2 NPs, and R_c is the radius of the bare SiO_2 NPs (=46.03 nm measured by DLS; DLS curves are shown in Figure S3 of the SI).[31-35] Both are hydrodynamic radii, although one is for bare NP and other is the particle with the PEG layer; as is well known these numbers do not match the TEM determined radius of the bare particles and the PEG-*g*-SiO_2, respectively.

Table 1. *Grafting density, molecular weight, radius of gyration, grafted chain number and brush height of the grafted PEG*

σ (chains /nm^2)[a]	M_n (g/mol)	R_g (nm)[b]	h (DLS, nm)[c]	Graft chains per particle [d]	h_{melt} (nm)[e]	x[f]	h_{dry} (nm)[g]
0.3	10k	3.8	10.3 ±0.2	2355	4.0	9.9	1.3
0.3	5k	3.0	6.5 ±1.0	2355	2.2	10.6	-0.2 (<0)
0.3	4k	2.4	4.8 ±0.2	2355	1.75	10.7	-0.5 (<0)
0.46	4k	2.4	4.9 ±1.5	3611	2.60	15.9	1.0
0.73	4k	2.4	7.9 ±2.1	5730	4.2	24.1	2.8

[a]Grafting density was determined by TGA.

[b]R_g is the average radius gyration of Gaussian chains in theta (Θ) conditions, and it can be calculated by $(N^*/6)^{1/2}l$, where l is the Kuhn length of PEO with a value of 1.1 nm[36] and N^* is the number of l segments in the PEO chains.

[c]Brush height is defined as $h = R_h - R_c$, where R_h is the hydrodynamic radius of the PEG-*g*-SiO_2 nanoparticles, and R_c is the radius of bare SiO_2 nanoparticles.

[d]Number of grafted chain number per NP was calculated by $Z = 4\pi R_c^2\sigma$.

[e]h_{melt} represents the brush height in the melt state.

[f] x is the overcrowding parameter.

[g] h_{dry} is the estimate of the dry layer thickness in the two layer[37] model. Values less than 0 imply that the model is outside its realm of validity. In these cases, it is likely that no dry region exists.

Because the results above results are in solution, a better way to track the brush height and the extent of chain overcrowding that leads to brush extension in the melt state is necessary. In recent work, Midya et al.[37] proposed that the brush height in a melt of PGNPs, h_{melt}, follows from the volume conservation equation:

$$\frac{4}{3}\pi(R_c + h_{melt})^3 = \frac{4}{3}\pi R_c^{\,3} + 4\pi R_c^{\,2}\sigma\frac{N}{\rho} \quad (1)$$

where R_c is the NP core radius (= 25 nm), N is the chain length and ρ is the monomer density. This equation assumes that the effective volume occupied by the PGNP equals the volume of the core and the polymeric corona. This work has also shown that the parameter that controls chain extension is an overcrowding parameter defined as

$$x = \frac{4R_c^2\sigma}{\rho_K b^2(R_c + h_{melt})} \quad (2)$$

where b is the Kuhn length of the chains (and hence ρ_K represents the density in units of Kuhn monomers per unit volume; note that this is smaller than the monomer density, ρ, by a factor that accounts for the number of monomers per Kuhn segment).

In addition, the last column in Table 1 corresponds to the height of the inner, dry brush (h_{dry})[37] where the chains are so stretched that they do not interpenetrate with chains grafted to other NPs. The dry layer thickness is given by $h_{dry} = h_{melt} - h_{inter}/2$, where h_{inter} is the thickness of an interpenetration layer that can be obtained through the equation:

$$h_{inter} = 3(R_c + h_{melt})(1+x)\left[1 - \sqrt{1 - \frac{4}{3}\left(\frac{1}{1+x}\right)^2}\right] \quad (3)$$

While three of the samples show positive values of h_{dry}, there are two samples with negative h_{dry} – the two layer model is not valid for these samples, likely because the chains are too short. Thus, regardless of the large x values, the negative h_{dry} implies that the grafted chains are too short to exclude chains from adjacent NPs; hence, we are likely in a regime where the matrix can interpenetrate the brush even

though the x values are large. Thus, the NP dispersion state (which we interchangeably call miscibility data) of these two samples likely represents an interplay of two factors: (i) the entropy of mixing between the matrix and the brush, which is favored for short chain matrices, but becomes less favorable for larger matrix chain lengths; (ii) the chains do not energetically prefer the silica surface (Figure 1b, discussed below). So, we expect that with increasing *P/N* the NPs will become significantly less compatible with the matrix.

The opposite case where $x >> 1$ and $h_{dry} > 0$ is easier to understand – in these cases the graft chains are strongly overcrowded, and hence strongly stretched and not interpenetrated with chains from adjacent NPs. In this limit of high overcrowding, our previous work has shown that there are really only two spatially accessible NP dispersion states: well-dispersed and aggregated [38] with the transition to phase separated (i.e., aggregated) states occurring for large *P/N*.

3.2.The dispersion state of PEO-*g*-SiO_2 NPs in the PEO matrix

To gain more insights into the dispersion state of the grafted NPs in PNCs, a combination of transmission electron microscopy (TEM) and small-angle X-ray scattering techniques (SAXS) was applied.[7, 39] TEM provides real space image evidence of NP dispersion over a limited (microscopic) area, while SAXS is the most effective method to assess larger sample areas. A strong upturn in the low-q region of the SAXS curves is usually interpreted as phase-separation or aggregation, with these phenomenon occurring on size scales outside the resolution of the SAXS

experiment.[40] In contrast, a plateau in the low-q region represents a well-dispersed state in PNCs.[39]

Figure 1a shows the SAXS and SAXS curves of different PEO/PEG-*g*-SiO_2 nanocomposites with 24 wt % SiO_2 content while Figure 1b shows the corresponding TEM images. The sample with 1700PEO/PEG4k-*g*-SiO_2-0.73 (1700 PEO represents the molecular weight of the matrix in g/mol) and the highest σ = 0.73 chains/nm^2 at *P/N* = 0.425 shows good dispersion of the NPs. Its low q scattering only rises slowly with decreasing q consistent with this conclusion. These findings are consistent with the 1700PEO/PEG10k-*g*-SiO_2-0.3 with the longest grafted PEG chain length M_n = 10k g·mol^{-1} at *P/N* = 0.17 (Figure 1a).

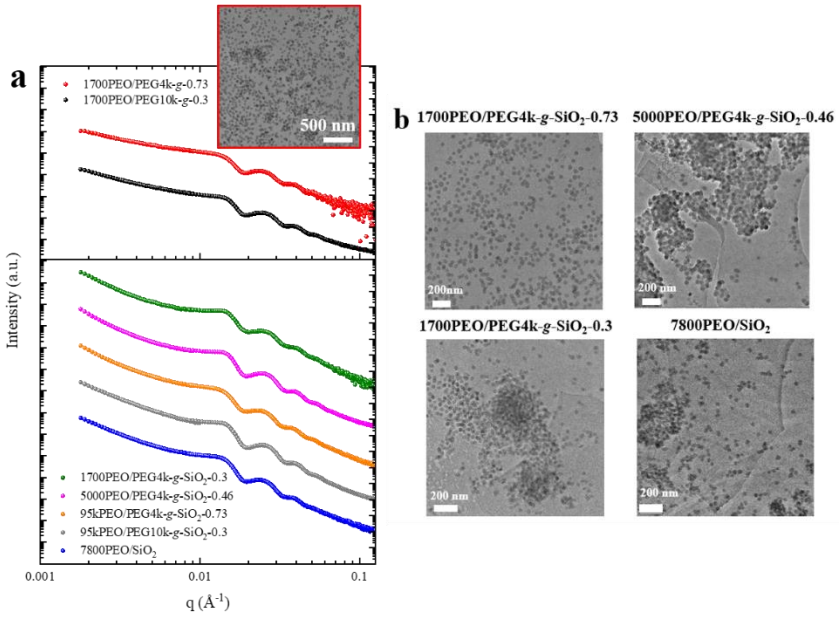

Figure 1. (a) SAXS curves of different PEO/PEG-g-SiO_2 nanocomposites with 24 wt % SiO_2. The SAXS curves are arbitrarily shifted for clarity. The insert image is the micrograph of 1700PEO/PEG4k-g-SiO_2-0.73 with a scale of 500 nm (b) TEM images of PEO/PEG-g-SiO_2 and PEO/SiO_2 nanocomposites.

Actually, a nanocomposite comprised of 24 weight% (volume fraction of 14.2 % equivalently) of nanoparticles is not a dilute system and a structure factor must be

introduced to properly describe the interparticle correlations. To this end the SAXS curves was fitted using a sphere form factor and a paracrystalline structure factor for a face-centered cubic structure[41] (as shown in Figure S4). The paracrystal model agrees well with the TEM images, in which particles with high grafting density are loosely packed with a preferential separation distance.

The results lie within the "Well-Dispersed" particle region (WD) corresponding to the morphology diagram summarized by Kumar et al.[6] Since the $h_{dry} > 0$ in these cases, our results imply that the entropy of mixing short matrix chains with the brush dominate these physical situations. The interaction of the matrix chains with the silica surface plays no role in these systems, because the grafted layers are stretched enough to prevent any chains from penetrating them.

Bare SiO_2 NPs tend to form aggregates due to the incompatibility between organic and inorganic phases as indicated by the TEM images (Figure 1b) and the low q upturn in the SAXS curve (Figure 1a, blue curve). This is either caused by an energetic dislike between the silica NPs and PEO or a manifestation of preparation conditions; we have previously shown that the use of some solvents give rise to well-dispersed NPs in PEO.[19, 21] Solvents which energetically prefer the silica surface instead of the PEG give rise to agglomerated NPs, likely due to depletion attraction forces[42-45]. Regardless of its origins, it is clear that the effective interactions between the PEO matrix and silica surface are unfavorable under the preparation conditions we adopt.

While Figures 1a and 1b show that good NP dispersion results at high grafting

density are due to entropic effects as discussed above, all other samples tend to form larger, generally spherical aggregates, suggesting macroscopic phase separation/NP aggregation. These samples correspond to larger *P/N* at the high σ, and all the *P/N* considered at lower σ. According to our fitting results of the aggregated sample (5000PEO/PEG4k-*g*-SiO_2-0.46, as shown in Figure S5), we introduced a contribution of a power law ($I \sim q^{-D}$) [39-40, 46] with a dimension of D = 4, which means there exists a sharp boundary between the objects (presumably comprised of the agglomerated NPs) and the surroundings. We believe that these results are a direct manifestation of the macrophase separation/NP aggregation caused by the effective dislike between the PEO matrix chains and the NP surface (only relevant for systems where $h_{dry} < 0$) coupled to the immiscibility between the brush and the matrix chains as we increase *P/N* at a fixed σ. These results are consistent with several other studies which have shown that σ is an essential factor which affects the PNC dispersion state.[13, 39, 47-50]

Returning now to the large σ data, we note that there are only two states: well-dispersed or aggregated NPs. This is thought to be a reflection of the matrix "autophobically" dewetting[6] the brush for large *P/N*. The interesting point here is that for smaller 14 nm diameter NPs this transition is thought to occur for $P/N > 4$,[15] while for flat brushes (infinite diameter) this transition occurs for $P/N > 1/\sqrt{N}$.[48] Since we find phase separation (aggregation) for $\frac{P}{N} > 1$ for these large NPs, even when we have a dry brush, we argue that the shift in this transition from dispersed to aggregated states is a manifestation of the lower curvature of these larger NPs. The dependence of this entropically driven boundary on NP diameter is an open question,

although these results are in qualitative agreement with expectations. Regardless, the essential point here is that controlling the grafting density and the *P/N* allows us to access well-dispersed or phase separated NP structures. The consequences of these assemblies on crystallization behavior are studied next.

3.3. Crystallization behavior of PEO/PEG-*g*-SiO_2 nanocomposites

3.3.1.The effects of σ and P/N on the crystallization behavior of PEO/PEG-g-SiO_2

Our critical emphasis is on delineating the role of NP dispersion state on the crystallization properties of PEO/PEG-*g*-SiO_2 PNCs. Figures 2a-d summarize the effects of σ on the crystallization temperature (T_c) at *P/N* = 0.425, 1.25, 1.95 and 5, respectively. The DSC melting and cooling curves, on which these data are based, are shown in Figure S6 of the SI. Additionally, separate TGA experiments show that all the chains used in the grafting process are chemically bonded to the NP surface – we find less than 0.5% (by weight) of ungrafted chains after repeated washing of the grafted NPs before they are blended with the free (matrix) chains.[51]

For each fixed value of graft length and fixed *P/N*, the T_c of the PEO nanocomposites monotonically increases as σ increases (Figures 2a, 2b and 2d), but with no obvious changes in T_m (melting temperature, as shown in Figure S7 of SI). Further, we find increased T_c for the PEG grafted SiO_2 NPs, even relative to the neat PEO, in all cases where the particles are better dispersed. Since our previous work[21] has shown that the addition of the PGNPs reduces the growth rate of the polymer crystals, an increase in T_c must be reflective of an increased nucleation rate on NP

addition.

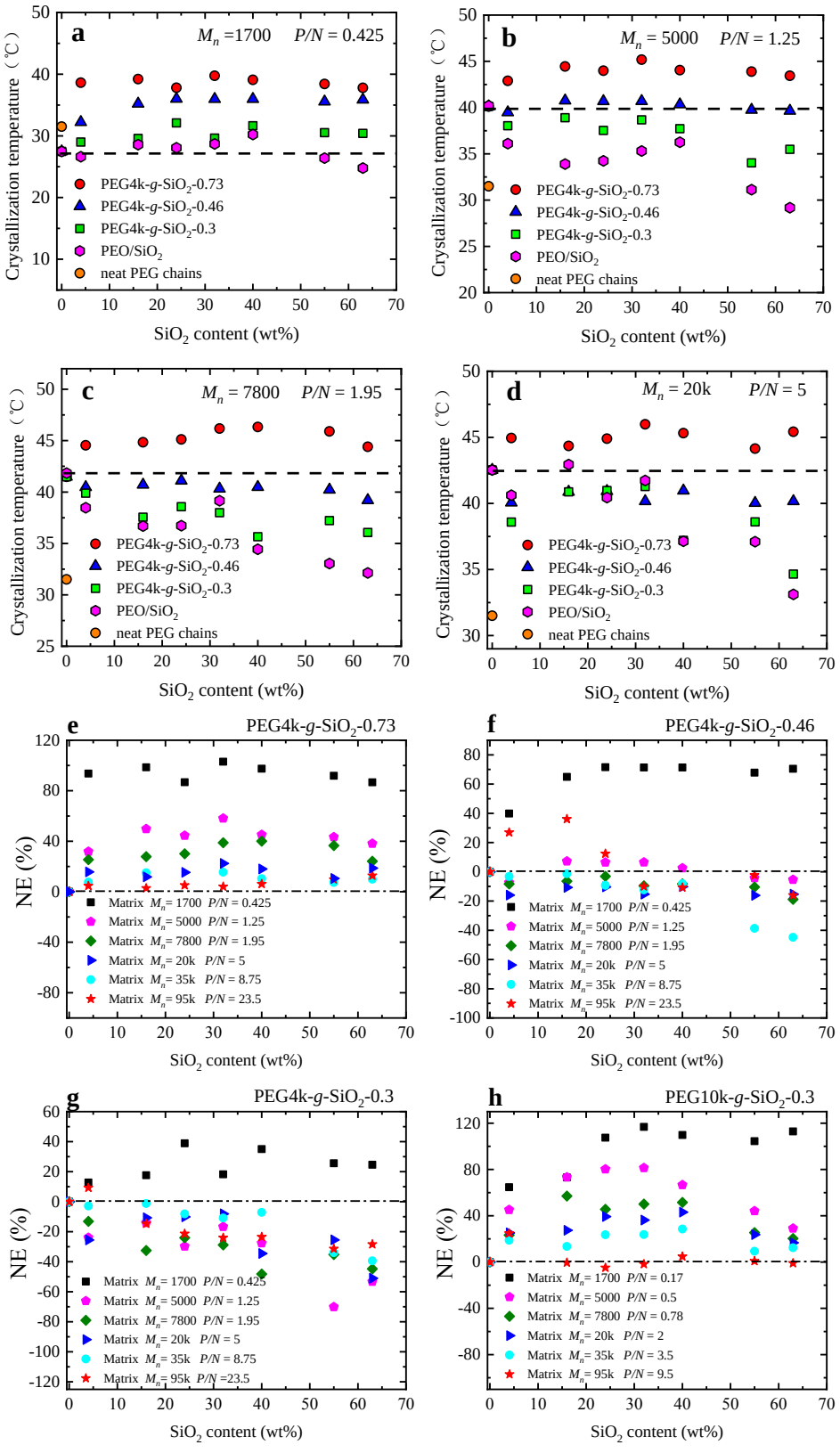
a
M_n =1700 P/N = 0.425
b
M_n = 5000 P/N = 1.25
c
M_n = 7800 P/N = 1.95
d
M_n = 20k P/N = 5
PEG4k-g-SiO$_2$-0.73
PEG4k-g-SiO$_2$-0.46
PEG4k-g-SiO$_2$-0.3
PEO/SiO$_2$
neat PEG chains
Crystallization temperature (℃)
SiO$_2$ content (wt%)
e
PEG4k-g-SiO$_2$-0.73
f
PEG4k-g-SiO$_2$-0.46
g
PEG4k-g-SiO$_2$-0.3
h
PEG10k-g-SiO$_2$-0.3
NE (%)
Matrix M_n= 1700 P/N = 0.425
Matrix M_n= 5000 P/N = 1.25
Matrix M_n= 7800 P/N = 1.95
Matrix M_n= 20k P/N = 5
Matrix M_n= 35k P/N = 8.75
Matrix M_n= 95k P/N =23.5
Matrix M_n= 1700 P/N = 0.17
Matrix M_n= 5000 P/N = 0.5
Matrix M_n= 7800 P/N = 0.78
Matrix M_n= 20k P/N = 2
Matrix M_n= 35k P/N = 3.5
Matrix M_n= 95k P/N = 9.5

Figure 2. *(a-d) Crystallization temperature of PEO/PEG-g-SiO_2 nanocomposites with three different grafting densities at P/N = 0.425,1.25,1.95 and 5, respectively. The "neat PEG chains"label means PEG homopolymers with the same M_n as those PEG chains grafted to SiO_2. The dotted line represents the crystallization temperature of neat PEO. (e-h) Nucleation efficiency of PEO/PEG-g-SiO_2 nanocomposites for different P/N values at each fixed grafting density: (e)PEG4k-g-SiO_2-0.73; (f) PEG4k-g-SiO_2-0.46; (g) PEG4k-g-SiO_2-0.3 and (h) PEG10k-g-SiO_2-0.3.*

Figures 2a and 2b show that PEG-*g*-SiO_2 NPs with the dry brush layers, i.e., the two higher σ, are more effective as nucleating agents than bare SiO_2 NPs over the full range of silica loadings. In comparison, the NPs without dry layers appear comparable to the PEO/bare silica nanocomposites and show reductions in T_c relative to the neat PEO, especially where the brush and matrix become less miscible (higher *P/N* ratio). At a given *P/N* nucleation effects follow the order: PEG-*g*-SiO_2-0.73 > PEG-*g*-SiO_2-0.46 > PEG-*g*-SiO_2-0.3 $\approx$ PEO/SiO_2. In the case of *P/N* = 0.425 with σ = 0.73 chains/nm^2 (i.e., the highest value), the T_c increased almost 12 ℃ compared to neat PEO (Figure 2a). This sample has better NP dispersion according to the SAXS results shown in Figure 1a.

It is evident that the variation of T_c is not only related to σ but is also dependent on *P/N*. Figures 2a-d show that the T_c of PEO/ PEG-*g*-SiO_2 nanocomposites decreases with an increase of *P/N* at fixed σ. When *P/N* increases to 1.25, there is almost no further enhancement of the crystallization temperature for 5000PEO/PEG4k-*g*-SiO_2-0.46 nanocomposites, and the T_c reaches values that are close to those of neat PEO (Figure 2b). It appears that the crystallinity (X_c) of the PEO matrix is significantly enhanced by the addition of PEG-*g*-SiO_2 with low molecular weight grafts (*P/N* = 0.425) as shown in Figure S8. With further increase in *P/N*, X_c is

observed to decrease as compared to the neat PEO. In the case of the lowest σ in 5000PEO/PEG4k-*g*-SiO_2-0.3, the crystallization of the nanocomposites is strongly hindered, and T_c is lower than the corresponding value of neat PEO over the entire range of SiO_2 content at *P/N* =1.25 (as shown in Figure 2b). The decrease of the T_c for PEO nanocomposites at lower σ and larger *P/N* may be closely related to the aggregation of PEG-*g*-SiO_2 in PEO nanocomposites, and the fact that the silica surface is now exposed to the matrix chains. In these cases we obtain results very similar to those obtained previously by Jimenez et al in the case of bare silica surfaces.[21]

In our previous study, we also showed that PEO-grafted-SiO_2 NPs resulted in a marked enhancement in the crystallization rate of PEO and increased nucleation with increases in grafting density.[52] The results presented in Figure 2, therefore, indicate that the hairy PEG-*g*-NPs with more stretched conformations of the grafted crystallizable PEG chains (with the increase of σ) can induce nucleation.

Our results, however, are different from the study of Jimenez et al.[19], in which the nucleation of PEO was practically unaffected by the addition of PMMA-grafted NPs (PMMA-*g*-SiO_2) even with variations of σ. In their case, PMMA chains cannot be included in the PEO crystal lattice even though PMMA is miscible with PEO in the melt state. Also, the PEO interacted favorably with their silica NPs.

The exact origin of such different nucleation behavior is not clear. We speculate that the strongly stretched grafted crystallizable chains, coupled to a wetting brush-interface, allows the matrix PEO chains to be templated by the surface chains,

whose conformational states are close in spirit to the crystal structure of the PEO. It is also possible that the PEO chains on the NPs can either be incorporated into the bulk PEG crystals. On this basis, then it is clear that nucleation enhancement in Figure 2 is correlated with better NP dispersion and higher graft densities of a crystallizable polymer.

To provide a more in-depth evidence of the PEO crystallization over a wide *P/N* range, we change the *P/N* value at each fixed σ. Moreover, to make a comprehensive comparison of the PEG-*g*-SiO_2 nucleation ability in different PEO matrices, the nucleation efficiency (*NE*) of PEG-*g*-SiO_2 was calculated based on the method devised by Fillon et al[53-54]. The *NE* can be obtained through the equation:

$$NE = 100\frac{T_{cNA} - T_{c1}}{T_{c2\max} - T_{c1}} \quad (4)$$

where T_{cNA} is the crystallization temperature of polymers which incorporates the foreign nucleating agents. T_{c1} is the crystallization temperature of the neat polymer, and the T_{c2max} is the maximum crystallization peak of polymers after being self-nucleated and annealed[55-56] (shown in Figure S9 of SI).

Figures 2e-h show the variation of *NE* in PEO/PEG-*g*-SiO_2 nanocomposites as a function of *P/N*. The range of *NE* values is remarkable, as they encompass from antinucleation (*NE*<0, see Figure 2g) to supernucleation (*NE*>100, see Figure 2h).[57-58] Supernucleation effects have been reported for different nanocomposites when the nucleating action of the nanofiller has a larger efficiency than the self-nuclei of the polymer under study.[57-58] These extreme changes in NE demonstrate the surprising control that carefully choosing the molecular parameters in these PNCs can have over

the nucleation process. The results indicate that *P/N* plays a crucial role in the crystallization of PEO nanocomposites. For PEO nanocomposites containing PEG4k-*g*-SiO_2-0.73 (Figure 2e), *NE* decreases with increasing *P/N*, and the increases of *NE* almost disappear when *P/N* increases to 23.5. For PEG4k-*g*-SiO_2-0.46 and PEG4k-*g*-SiO_2-0.3, the most significant nucleation effects can be observed at *P/N* = 0.425 in Figures 2f-g. Our results are also in accordance with the previous study of Zhao et al.[52] who found a marked enhancement in the crystallization ability of PEO when PEO grafted SiO_2 NPs are added at a lower *P/N* = 0.8, although the grafted SiO_2 disperses poorly in the PEO matrix in their case.[52] With further increases in *P/N*, the presence of PEG-*g*-SiO_2 exhibits an anti-nucleation effect, i.e., *NE* < 0 (Figures 2f-g). We speculate that at low σ the aggregation of PGNPs coupled to the fact that the silica surface is now exposed to the PEO chains, play major roles in suppressing PEO nucleation with increasing *P/N*.

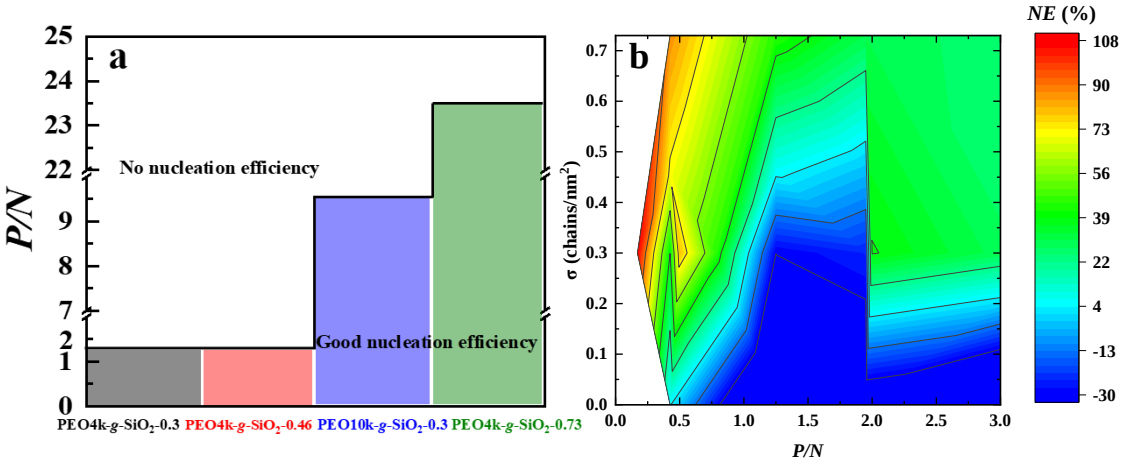

Figure 3. (a) Critical points of P/N for nucleation efficiency of PEO nanocomposites with different PEG-g-SiO_2. (b) Contour plot of the nucleation efficiency changes with the variation of σ and. The particle concentration is φ_{SiO2} = 24 wt %.

To concisely capture the effects of *P/N* on the crystallization behavior of PEO nanocomposites, Figure 3a illustrates the critical points (i.e., the values at which the *NE* changes from positive to negative) of *P/N* for *NE* for the four different PEO nanocomposites. Compared to the case where PNCs contain the highest PEG-*g*-SiO_2 σ value (PEO/PEG4k-*g*-SiO_2-0.73), the *P/N* critical point for positive nucleation efficiency decreases from *P/N* = 23.5 to *P/N* = 1.25 at lower σ (as PEO/PEG4k-*g*-SiO_2-0.46 and PEO/PEG4k-*g*-SiO_2-0.3). The critical value of *P/N* increases with the increase of σ and with the grafted chain length.

Consequently, to obtain a better understanding of the overall crystallization process with the variation of both σ and *P/N*, the above results were replotted as a contour map in Figure 3b. This plot further confirms that the *NE* of PEO nanocomposites is significantly enhanced with increases of σ and decreases of *P/N* (the red colored region in Figure 3b). Combined with the SAXS results, we conclude that PEG-*g*-SiO_2 at higher σ and lower *P/N* can significantly improve both the dispersion and the overall crystallization in PNCs (via nucleation enhancement).

3.3.2. Nucleation densities in the crystallization process of PEO/PEG-g-SiO_2 nanocomposites

The addition of PGNPs can readily improve the dispersion state of PNCs for certain σ and *P/N* ranges. Such improvement can, in some cases, significantly increase nucleation density and thus enhance overall crystallization.[59-60]

To probe this issue further, we use polarized light optical microscopy (PLOM) to

measure the nucleation density of our PEO nanocomposites (Figure 4). As described above, our emphasis is on the non-isothermal crystallization of PEO nanocomposites. Thus, the PLOM were made under similar conditions as the DSC measurements.

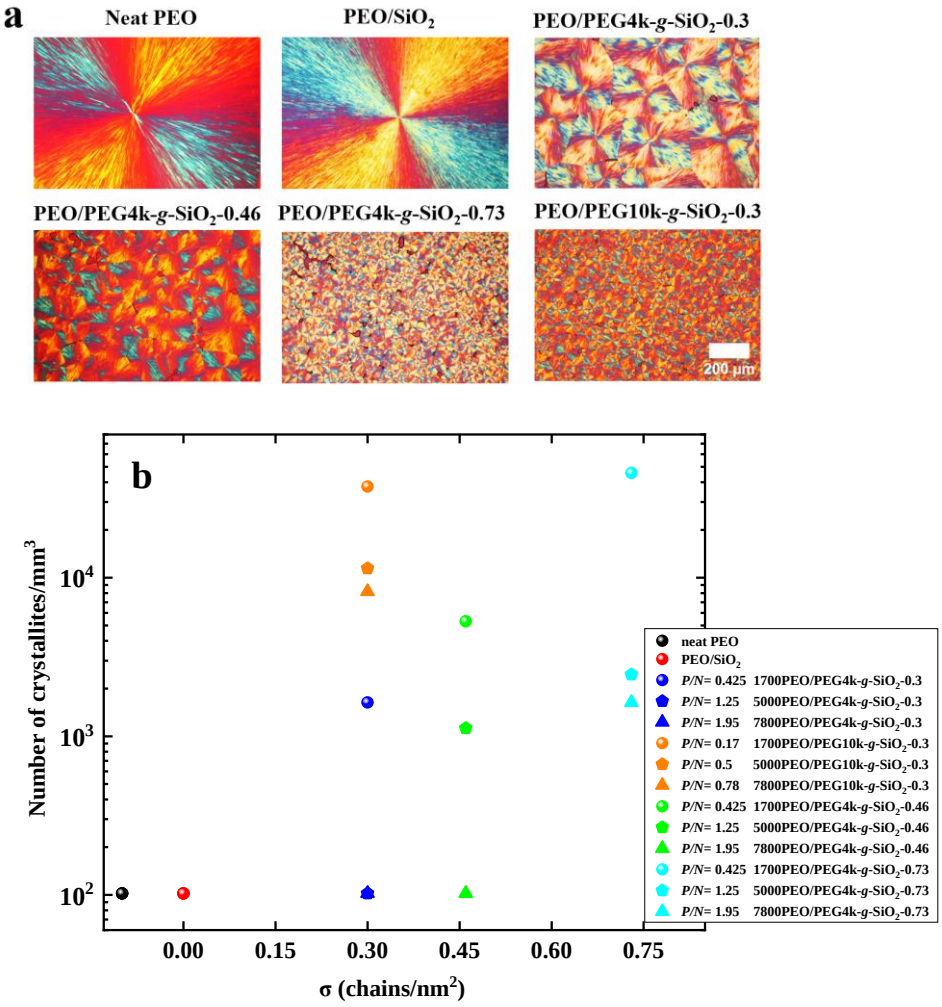

Figure 4. (a) PLOM images of PEO/PEG-g-SiO_2 with different grafting density mixed with PEO matrix of M_n=1700 g/mol. (b) Changing tendency of nucleation density with grafting density and grafting molecular weight.

Figure 4a shows the spherulitic morphology of PNCs with the PEO matrix of M_n = 1700 g/mol as an example, taken at 25 ℃ after cooling from the melt (i.e., 100 ℃) at a rate of 20 ℃/min. Several nuclei are observed for neat PEO and PEO/SiO_2. The enhanced nucleation ability of several of the PEG-*g*-SiO_2 NPs can also be clearly

observed. The nucleation density increases with σ values and decreases with *P/N*. This result is consistent with the DSC-based analysis above. The good compatibility between PEG-*g*-SiO_2 and the PEO matrix at high σ (1700PEO/PEO4k-*g*-SiO_2-0.73) and low *P/N* (1700PEO/PEO10k-*g*-SiO_2-0.3) enhances the interaction between PEO chains and PEG-*g*-SiO_2 NPs, thus improving the NP dispersion. Such dispersion improvement appears to be the key for the enhancement in nucleation density observed in Figure 4a. For brevity, Figure 4b shows the spherulitic density (directly proportional to the nucleation density) of the PEO PGNPs. The nucleation density exhibits larger values for high σ and low *P/N*.

The morphological evolution of PEO nanocomposites with larger molecular weight PEO matrices (i.e., with increases in *P/N*) is reported in Figure S10. This figure clearly shows that for the low σ systems, increasing *P/N* has a notable impact on the variation of nucleation density. Nucleation density appears similar to that of neat PEO when *P/N* increases to 1.25 for 5000PEO/PEG4k-*g*-SiO_2-0.3 and 1.95 for 7800PEO/PEG4k-*g*-SiO_2-0.46 (as shown in Figure 4b). In the case of low σ, the NPs distribution is more sensitive to changes in *P/N*. As aggregation occurs at large *P/N* values, it further limits the effectiveness of grafted PEG NPs on the nucleation of the PNCs, and the nucleation density is significantly reduced.

Taking into account the results obtained, Figure 5 presents a schematic model of the morphology for PEG-*g*-SiO_2 NPs within the PEO matrix with respect to the variation of σ and *P/N*. In the case of lower σ and larger *P/N* values, matrix PEO chains are likely excluded from the grafted layer and the PEO-*g*-SiO_2 NPs tend to

form aggregates. This leads to the suppression of nucleation in the PEO nanocomposites (Figure 5a). With increasing σ and decreasing *P/N*, the more stretched structure of grafted PEG chains induces a better dispersion of PEG-*g*-SiO_2 NPs within the PEO matrix. The extended PEG graft chains may act as a template causing an increase of nucleation sites that enhance overall crystallization (shown in Figure 5b). Further increases in σ and decreases in *P/N* values cause further stretching of the grafted PEG chains away from the SiO_2 surface enhancing nanoparticle dispersion, nucleation and overall crystallization (Figure 5c).

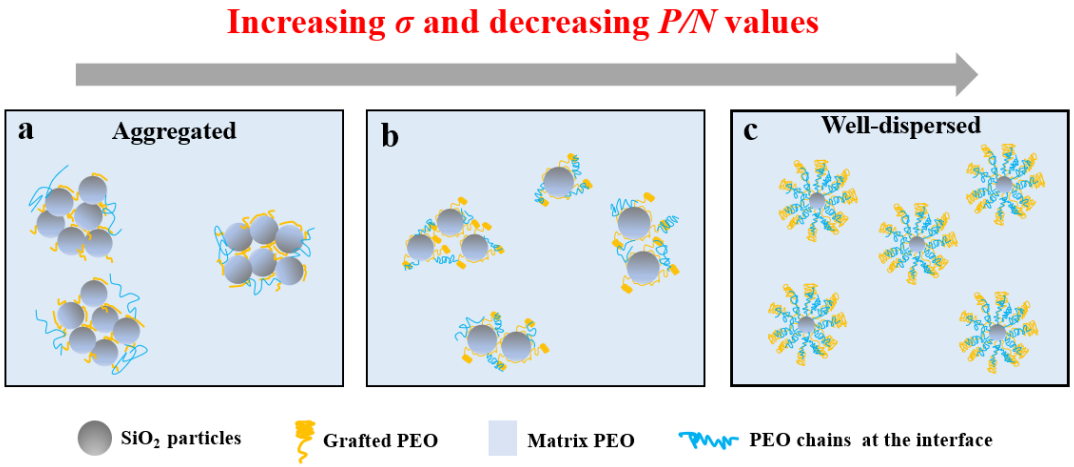

Figure 5. Schematic illustration of PEO/PEG-g-SiO_2 nanocomposites

4. CONCLUSIONS

We have systematically studied the effects of changing σ and *P/N* on the crystallization behavior of PEO/PEG-*g*-SiO_2 nanocomposites by DLS, SAXS, DSC and PLOM techniques. Compared to the bare SiO_2, the addition of PEG-*g*-SiO_2 in the PEO matrix can result in enhanced nucleation. Variations of σ and *P/N* significantly affect the dispersion state of the NPs, which in turn determines the crystallization

ability of PEO nanocomposites. Well-dispersed PEG-*g*-SiO_2 NPs with more stretched chains provide more nucleation sites with the increase of σ and the decrease of *P/N*, which markedly enhance the crystallization of PEO nanocomposites. Moreover, the nucleation efficiency of PEO nanocomposites is highly enhanced at high σ and low *P/N* value. We thus argue that NPs grafted with crystallizable polymers show enhanced nucleation capability, especially in the limit where they have extended brushes but are still miscible with the crystallizable matrix. These results are quite evidently different from those obtained from bare silica NPs or NPs grafted with amorphous brushes, where such templating effects are obviously suppressed. Thus, we believe that the nature of the graft chains plays a crucial role in the crystallization behavior of semicrystalline polymer nanocomposites.

ASSOCIATED CONTENT

Supporting Information. TGA details. DLS details. TEM details. DSC details and additional information on self-nucleation technique. PLOM details. SAXS fitting data.

The Supporting Information is available free of charge.

Figures S1−S10 (PDF).

AUTHOR INFORMATION

Corresponding Author

*E-mail ylsu@iccas.ac.cn and alejandrojesus.muller@ehu.es

Notes

The authors declare no competing financial interest.

ACKNOWLEDGMENTS

This project is supported by the Ministry of Science and Technology of China (2017YFE0117800) and the National Natural Science Foundation of China (21574141). We would like to thank the financial support provided by the BIODEST project; this project has received funding from the European Union's Horizon 2020 research and innovation programme under the Marie Skłodowska-Curie grant agreement No 778092. The authors thank Prof. Yongfen Men (CIAC) for providing the SAXS beam time and helps during experiments. The discussion of TEM data with Andrew M. Jimenez (Columbia University, New York, NY) is gratefully acknowledged. We also thank B. Guan, J. L. Yue and K. A. Liu for help in cryo-TEM experiments.

References

1. Honma, I.; Nomura, S.; Nakajima, H. Protonic conducting organic/inorganic nanocomposites for polymer electrolyte membrane. *J. Membr. Sci.* **2001,** *185*, 83−94.

2. Zhao, W. W.; Su, Y. L.; Wang, D. J. Synergetic effects of interfacial and spatial confinement in polymer nanocomposites. *Mod. Phys. Lett. B* **2017,** *31*, 1730003.

3. Rong, M. Z.; Zhang, M. Q.; Ruan, W. H. Surface modification of nanoscale fillers for improving properties of polymer nanocomposites: A review. *Mater. Sci. Technol.* **2006,** *22*, 787−796.

4. Wu, X. Y.; Zhang, H. B. Study on structure design and electromagnetic shielding properties of polymer nanocomposites. *Acta Polym. Sin.* **2020,** *51*, 573−585.

5. Imtiaz, S.; Siddiq, M.; Kausar, A.; Muntha, S. T.; Ambreen, J.; Bibi, I. A review featuring fabrication, properties and applications of carbon nanotubes (CNTs) reinforced polymer and epoxy nanocomposites. *Chin. J. Polym. Sci.* **2018,** *36*, 445−461.

6. Kumar, S. K.; Jouault, N.; Benicewicz, B.; Neely, T. Nanocomposites with polymer grafted nanoparticles. *Macromolecules* **2013,** *46*, 3199−3214.

7. Srivastava, S.; Agarwal, P.; Archer, L. A. Tethered nanoparticle-polymer composites: phase stability and curvature. *Langmuir* **2012,** *28*, 6276−6281.

8. Akcora, P.; Kumar, S. K.; Moll, J.; Lewis, S.; Schadler, L. S.; Li, Y.; Benicewicz, B. C.; Sandy, A.; Narayanan, S.; Illavsky, J.; Thiyagarajan, P.; Colby, R. H.; Douglas, J. F. "Gel-like" mechanical reinforcement in polymer nanocomposite melts. *Macromolecules* **2010,** *43*, 1003−1010.

9. Chen, X. C.; Green, P. F. Control of morphology and its effects on the optical properties of polymer nanocomposites. *Langmuir* **2010,** *26*, 3659−3665.

10. Moraes, J.; Ohno, K.; Maschmeyer, T.; Perrier, S. Synthesis of silica-polymer core-shell nanoparticles by reversible addition-fragmentation chain transfer polymerization. *Chem. Commun.* **2013,** *49*, 9077−9088.

11. Lan, Q.; Francis, L. F.; Bates, F. S. Silica nanoparticle dispersions in homopolymer versus block copolymer. *J. Polym. Sci., Part B: Polym. Phys.* **2007,** *45*, 2284−2299.

12. Jouault, N.; Vallat, P.; Dalmas, F.; Said, S.; Jestin, J.; Bouéé, F. Well-dispersed fractal aggregates as filler in polymer-silica nanocomposites: Long-range effects in rheology. *Macromolecules* **2009,** *42*, 2031−2040.

13. Green, P. F. The structure of chain end-grafted nanoparticle/homopolymer nanocomposites. *Soft Matter* **2011,** *7*, 7914−7926.

14. Xu, C.; Ohno, K.; Ladmiral, V.; Composto, R. J. Dispersion of polymer-grafted magnetic nanoparticles in homopolymers and block copolymers. *Polymer* **2008,** *49*, 3568−3577.

15. Chevigny, C.; Dalmas, F.; Di Cola, E.; Gigmes, D.; Bertin, D.; Bouéé, F.; Jestin, J. Polymer-grafted-nanoparticles nanocomposites: dispersion, grafted chain conformation, and rheological behavior. *Macromolecules* **2011,** *44*, 122−133.

16. Wen, X. N.; Zhao, W. W.; Su, Y. L.; Wang, D. J. Interfacial effects on crystallization behavior of polymer nanocomposites with polymer-grafted nanoparticles. *Polymer Crystallization* **2019**, e10066.

17. Bieligmeyer, M.; Taheri, S. M.; German, I.; Boisson, C.; Probst, C.; Milius, W.; Altstadt, V.; Breu, J.; Schmidt, H. W.; D'Agosto, F.; Forster, S. Completely miscible polyethylene nanocomposites. *J. Am. Chem. Soc.* **2012,** *134*, 18157−18160.

18. Wu, F.; Zhang, S. Y.; Zhang, B.; Yang, W.; Liu, Z. Y.; Yang, M. B. The effect of the grafted chains on the crystallization of PLLA/PLLA-grafted SiO2 nanocomposites. *Colloid Polym Sci.* **2016,** *294*, 801−813.

19. Jimenez, A. M.; Krauskopf, A. A.; Pérez-Camargo, R. A.; Zhao, D.; Pribyl, J.; Jestin, J.; Benicewicz, B. C.; Müller, A. J.; Kumar, S. K. Effects of hairy nanoparticles on polymer crystallization kinetics. *Macromolecules* **2019,** *52*, 9186−9198.

20. Zhao, D.; Gimenez-Pinto, V.; Jimenez, A. M.; Zhao, L. X.; Jestin, J.; Kumar, S. K.; Kuei, B.; Gomez, E. D.; Prasad, A. S.; Schadler, L. S.; Khani, M. M.; Benicewicz, B. C. Tunable multiscale nanoparticle ordering by polymer crystallization. *ACS Central Sci.* **2017,** *3*, 751−758.

21. Jimenez, A. M.; Al-Torbaq, A. S.; Müller, A. J.; Kumar, S. K. Polymer crystallization under confinement by well-dispersed nanoparticles. *Macromolecules* **2020,** *53*, 10256−10266.

22. Altorbaq, A.; Jimenez, A. M.; Pribyl, J.; Benicewicz, B. C.; Müller, A. J.; Kumar, S. K. Polymer spherulitic growth kinetics mediated by nanoparticle assemblies. *Submitted to Macromolecules.*

23. Hong, B. B.; Panagiotopoulos, A. Z. Molecular dynamics simulations of silica nanoparticles grafted with poly(ethylene oxide) oligomer chains. *J. Phys. Chem. B* **2012,** *116*, 2385−2395.

24. Grunewald, T. A.; Lassenberger, A.; van Oostrum, P. D. J.; Rennhofer, H.; Zirbs, R.; Capone, B.; Vonderhaid, I.; Amenitsch, H.; Lichtenegger, H. C.; Reimhult, E. Core-shell structure of monodisperse poly(ethylene glycol)-grafted iron oxide nanoparticles studied by small-angle X-ray scattering. *Chem. Mater.* **2015,** *27*, 4763−4771.

25. Aranda, P.; Ruizhitzky, E. Poly(ethylene oxide)-silicate intercalation materials. *Chem. Mater.* **1992,** *4*, 1395−1403.

26. Rissanou, A. N.; Papananou, H.; Petrakis, V. S.; Doxastakis, M.; Andrikopoulos, K. S.; Voyiatzis, G. A.; Chrissopoulou, K.; Harmandaris, V.; Anastasiadis, S. H. Structural and conformational properties of poly(ethylene oxide)/silica nanocomposites: Effect of confinement. *Macromolecules* **2017,** *50*, 6273−6284.

27. Chen, G. X.; Kim, H. S.; Park, B. H.; Yoon, J. S. Controlled functionalization of multiwalled carbon nanotubes with various molecular-weight poly(L-lactic acid). *J. Phys. Chem. B* **2005,** *109*, 22237−22243.

28. StÖber, W.; Fink, A. Controlled growth of monodisperse silica spheres in the micron size range. *J. Colloid Interface Sci.* **1968,** *26*, 62−69.

29. Wen., X. N.; Su., Y. L.; Shui., Y. D.; Zhao., W. W.; Müller., A. J.; Wang., D. J. Correlation between grafting density and confined crystallization behavior of poly(ethylene glycol) grafted to silica. *Macromolecules* **2019,** *52*, 1505−1516.

30. Dukes, D.; Li, Y.; Lewis, S.; Benicewicz, B.; Schadler, L.; Kumar, S. K. Conformational transitions of spherical polymer brushes: Synthesis, characterization, and theory. *Macromolecules* **2010,** *43*, 1564−1570.

31. Kim, C. J.; Sondergeld, K.; Mazurowski, M.; Gallei, M.; Rehahn, M.; Spehr, T.; Frielinghaus, H.; Stuhn, B. Synthesis and characterization of polystyrene chains on the surface of silica nanoparticles: Comparison of SANS, SAXS, and DLS results. *Colloid Polym. Sci.* **2013,** *291*, 2087–2099.

32. Zdyrko, B.; Varshney, S. K.; Luzinov, I. Effect of molecular weight on synthesis and surface morphology of high-density poly(ethylene glycol) grafted layers. *Langmuir* **2004,** *20*, 6727−6735.

33. Iyer., K. S.; Luzinov., I. Effect of macromolecular anchoring layer thickness and molecular weight on polymer grafting. *Macromolecules* **2004,** *37*, 9538−9545.

34. Zdyrko, B.; Klep, V.; Luzinov, I. Synthesis and surface morphology of high-density poly(ethylene glycol) grafted layers. *Langmuir* **2003,** *19*, 10179−10187.

35. Hommel, H.; Legrand, A. P.; Tougne, P.; Balard, H.; Papirer, E. Influence of the grafting ratio on the conformations of poly(ethylene oxide) chains grafted on silica. *Macromolecules* **1984,** *17*, 1578−1581.

36. Maitra, P.; Ding, J.; Huang, H.; Wunder, S. L. Poly(ethylene oxide) silananted nanosize fumed silica: DSC and TGA characterization of the surface. *Langmuir* **2003,** *19*, 8994−9004.

37. Midya, J.; Rubinstein, M.; Kumar, S. K.; Nikoubashman, A. Structure of polymer-grafted nanoparticle melts. *ACS Nano* **2020,** *14*, 15505−15516.

38. Akcora, P.; Liu, H.; Kumar, S. K.; Moll, J.; Li, Y.; Benicewicz, B. C.; Schadler, L. S.; Acehan, D.; Panagiotopoulos, A. Z.; Pryamitsyn, V.; Ganesan, V.; Ilavsky, J.; Thiyagarajan, P.; Colby, R. H.; Douglas, J. F. Anisotropic self-assembly of spherical

polymer-grafted nanoparticles. *Nat. Mater.* **2009,** *8*, 354−359.

39. Sunday, D.; Ilavsky, J.; Green, D. L. A Phase diagram for polymer-grafted nanoparticles in homopolymer matrices. *Macromolecules* **2012,** *45*, 4007−4011.

40. Mangal, R.; Nath, P.; Tikekar, M.; Archer, L. A. Enthalpy-driven stabilization of dispersions of polymer-grafted nanoparticles in high-molecular-weight polymer melts. *Langmuir* **2016,** *32*, 10621−10631.

41. Matsuoka, H.; Tanaka, H.; Hashimoto, T.; Ise, N. Elastic-scattering from cubic lattice systems with paracrystalline distortion. *Phys. Rev. B.* **1987,** *36*, 1754−1765.

42. Jouault, N.; Zhao, D.; Kumar, S. K. Role of casting solvent on nanoparticle dispersion in polymer nanocomposites. *Macromolecules* **2014,** *47*, 5246−5255.

43. Harton, S. E.; Kumar, S. K. Mean-field theoretical analysis of brush-coated nanoparticle dispersion in polymer matrices. *J. Polym. Sci., Part B: Polym. Phys.* **2007,** *46*, 351–358.

44. Asakura, S.; Oosawa, F. On interaction between 2 bodies immersed in a solution of macromolecules. *J. Chem. Phys.* **1954,** *22*, 1255−1256.

45. Janes, D. W.; Moll, J. F.; Harton, S. E. Dispersion morphology of poly(methyl acrylate)/silica nanocomposites. *Macromolecules* **2011,** *44*, 4920−4927.

46. Mangal, R.; Srivastava, S.; Archer, L. A. Phase stability and dynamics of entangled polymer–nanoparticle compositestes. *Nat. Commun.* **2015,** *6*, 7198−7198.

47. Maillard, D.; Kumar, S. K.; Fragneaud, B.; Kysar, J. W.; Rungta, A.; Benicewicz, B. C.; Deng, H.; Brinson, L. C.; Douglas, J. F. Mechanical properties of thin glassy polymer films filled with spherical polymer-grafted nanoparticles. *Nano Letters* **2012,**

12, 3909−3914.

48. Ferreira, P. G.; Ajdari, A.; Leibler, L. Scaling law for entropic effects at interfaces between grafted layers and polymer melts. *Macromolecules* **1998,** *31*, 3994−4003.

49. Green, P. E.; Oh, H.; Akcora, P.; Kumar, S. K. Structure and dynamics of polymer nanocomposites involving chain-grafted spherical nanoparticles. In: Garc á Sakai V., Alba-Simionesco C., Chen SH. (eds) Dynamics of soft matter: Neutron applications. Springer, New York, NY. **2012**, 349−366.

50. Ndoro, T. V. M.; Voyiatzis, E.; Ghanbari, A.; Theodorou, D. N.; Bohm, M. C.; Muller-Plathe, F. Interface of grafted and ungrafted silica nanoparticles with a polystyrene matrix: atomistic molecular dynamics simulations. *Macromolecules* **2011,** *44*, 2316−2327.

51. Shui, Y. D.; Su, Y. L.; Kuang, X.; Zhao, W. W.; Cai, Y. L.; Wang, D. J. Facile and controllable synthesis of hybrid silica nanoparticles densely grafted with poly(ethylene glycol). *Polym. Int.* **2017,** *66*, 1395−1401.

52. Zhao, W. W.; Su, Y. L.; Wen, X. N.; Wang, D. J. Manipulating crystallization behavior of poly(ethylene oxide) by functionalized nanoparticle inclusion. *Polymer* **2019,** *165* 28−38.

53. Fillon, B.; Wittmann, J. C.; Lotz, B.; Thierry., A. Self-nucleation and recrystallization of isotactic polypropylene (a phase) investigated by differential scanning calorimetry. *J. Polym. Sci., Part B: Polym. Phys.* **1993,** *31*, 1383−1393.

54. Fillon, B.; Lotz, B.; Thierry, A.; Wittmann., J. C. Self-nucleation and enhanced nucleation of polymers. Definition of a convenient calorimetric “efficiency scale” and

evaluation of nucleating additives in isotactic polypropylene (a phase) *J. Polym. Sci., Part B: Polym. Phys.* **1993,** *31*, 1395−1405.

55. Michell, R. M.; Mugica, A.; Zubitur, M.; Müller, A. J. Self-nucleation of crystalline phases within homopolymers, polymer blends, copolymers, and nanocomposites. *Adv. Polym. Sci.* **2015,** *276*, 215−256.

56. Trujillo, M.; Arnal, M. L.; Müller, A. J.; Laredo, E.; Bredeau, S.; Bonduel, D.; Dubois, P. Thermal and morphological characterization of nanocomposites prepared by in-situ polymerization of high-density polyethylene on carbon nanotubes. *Macromolecules* **2007,** *40*, 6268−6276.

57. Müller, A. J.; Arnal, M. L.; Trujillo, M.; Lorenzo, A. T. Super-nucleation in nanocomposites and confinement effects on the crystallizable components within block copolymers, miktoarm star copolymers and nanocomposites. *Eur. Polym. J.* **2011,** *47*, 614–629.

58. Colonna, S.; Pérez-Camargo, R. A.; Chen, H. M.; Liu, G. M.; Wang, D. J.; Müller, A. J.; Saracco, G.; Fina, A. Supernucleation and orientation of poly(butylene terephthalate) crystals in nanocomposites containing highly reduced graphene oxide. *Macromolecules* **2017,** *50*, 9380–9393.

59. Xu, J. Z.; Zhang, Z. J.; Xu, H.; Chen, J. B.; Ran, R.; Li, Z. M. Highly enhanced crystallization kinetics of poly(L-lactic acid) by poly(ethylene glycol) grafted graphene oxide simultaneously as heterogeneous nucleation agent and chain mobility promoter. *Macromolecules* **2015,** *48*, 4891−4900.

60. Toyonaga, M.; Chammingkwan, P.; Terano, M.; Taniike, T. Well-defined

polypropylene/polypropylene-grafted silica nanocomposites: Roles of number and molecular weight of grafted chains on mechanistic reinforcement. *Polymers-Basel* **2016,** *8*, 300.

For Table of Contents use only